Focusing of High-Perveance Planar Electron Beams in a Miniature Wiggler Magnet Array

Stanley Humphries, *Fellow, IEEE*, Steven Russell, Bruce Carlsten, and Lawrence Earley

***Abstract*—The transport of planar electron beams is a topic of increasing interest for applications to high-power, high-frequency microwave devices. This paper describes two- and three-dimensional simulations of electron-beam transport in a notched wiggler magnet array. The calculations include self-consistent effects of beam-generated fields. The simple notched wiggler configuration can provide vertical and horizontal confinement of high-perveance sheet electron beams with small transverse dimensions. The feasibility calculations address a beam system to drive a 95-GHz traveling-wave tube experiment under construction at Los Alamos National Laboratory, Los Alamos, NM.**

***Index Terms*—Bean transport, charge-particle simulation, high-current beam, planar beam, wiggler magnet focusing.**

I. Introduction

THIS paper describes two-dimensional (2-D) and three-dimensional (3-D) simulations of the transport of high-perveance planar electron beams in a permanent-magnet wiggler array. Here, the term *planar* implies that the height of the beam (*vertical* direction) is much smaller than the width (*horizontal* direction). The studies have two novel features: 1) emphasis on miniature systems for small-dimension beams and 2) investigation of notched magnet faces to provide nonlinear wiggle plane focusing for intense beams. Planar beams are potentially useful for the generation of high-power microwave radiation in devices such as sheet-beam klystrons and high-frequency traveling-wave tubes [1]–[11], [22], [23]. Flat beams have several advantages for the application.

1) Higher net current can be transported for a given maximum focusing field.
2) The kinetic energy spread from space-charge effects is smaller.
3) The extended interaction area ensures smaller RF electric fields for a given power, reducing the possibility of breakdown.
4) Miniature RF structures (with scale size comparable to the beam height) can be used for high-frequency applications.

The last feature is critical for high-frequency traveling-wave tubes. The goal of the program [12], [13] at Los Alamos National Laboratory (LANL) is the efficient generation of megawatts of microwave radiation in the frequency range of 95 GHz. This frequency corresponds to a vacuum wavelength of only $\lambda = 3.2$ mm. An experiment under construction at the laboratory has the target beam parameters shown in Table I. In the table (and in the remainder of the paper), we apply the convention that the planar beam propagates in z, has large dimension in x and small dimension in y. We plan to create planar beams with the target parameters using a conventional circular-beam electron gun combined with a transformation system based on a solenoid lens with elliptical pole apertures (Fig. 1). Reference [14] describes properties of the lens and simulations of beam transport. The device produces approximately linear focusing forces with different focal lengths in x and y. The angular divergence value in Table I is set by the limitations of the optical system.

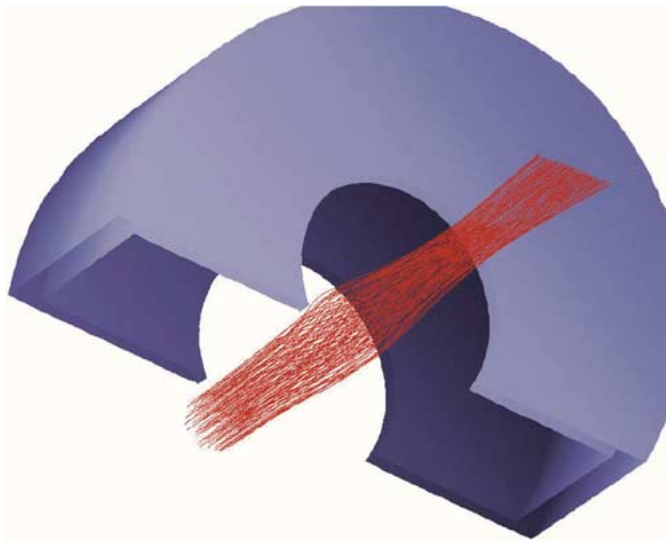

Fig. 1. Cutaway view of the pole-piece of an elliptical-aperture solenoid lens for circular-to-plane beam transformation. Red lines are orbits of selected model electrons to represent a 20 A, 120 keV beam with full effects of beam-generated electric and magnetic fields. Aperture is rotated to give a planar beam aligned with the x-y axes of the simulation.

Beam transport in the traveling-wave tube experiment poses several challenges. The vertical confinement forces must be strong enough to preserve the small height in the presence of space-charge forces and the relatively large emittance of the focused beam. Magnetic field strength in the wiggler is limited by the properties of available permanent-magnet materials, the minimum bore size and the maximum cell length of the periodic system. The bore size is constrained by the size of the traveling-wave structure, while the cell length is limited by orbital stability. The beam properties and required interaction length dictate that horizontal focusing is essential. Because of image-charge and current induced in the traveling-wave structure, the forces of beam-generated fields are concentrated at the envelope, even if the beam has an ideal elliptical cross

Manuscript received September 4, 2004; revised December 12, 2004.

S. Humphries is with Field Precision, Albuquerque, NM 87192 USA.

S. Russell, B. Carlsten, and L. Earley are with the Los Alamos National Laboratory, Los Alamos, NM 87545 USA.

Digital Object Identifier 10.1109/TPS.2005.845088

TABLE I
PARAMETERS OF THE LOS ALAMOS TWT EXPERIMENT

Quantity	Symbol	Value
Kinetic energy	T_e	120 keV
Current	I	20 A
Generalized perveance	K	6.16×10^{-3}
Full height of planar beam	$2y_o$	0.5 mm
Full width of planar beam	$2x_o$	10.0 mm
Planar beam vertical angular divergence	$\Delta\theta$	0.06 radian
Length of interaction region	L	> 10 cm

section. Therefore, we seek a focusing system that provides appropriate nonlinear forces.

Section II reviews vertical confinement in a wiggler and the mechanism of edge focusing in an array with notched pole faces. Section III describes 2-D simulations of beam matching and vertical focusing, including effects of emittance and self-consistent beam forces. We investigated ideal arrays as well as systems with random errors in remanence field and magnet thickness. The calculations confirm that: 1) the requirements of the LANL system can be met with existing magnet materials and that 2) individual magnets must have properties that are uniform to within a few percent to prevent to growth of envelope oscillations. Section III summarizes results of 3-D simulations of intense planar beams in a notched wiggler. The calculations demonstrate that the nonlinear edge focusing forces can maintain the required height and width of the planar beam over an extended interaction length with little distortion of the profile.

II. WIGGLER FOCUSING BASICS

A wiggler [15] consists of upper and lower stacks of permanent magnets with opposing magnetization direction, as shown in Fig. 2 (note that the figure shows only the portion above the symmetry boundary at $y = 0.0$). To begin, we limit attention to vertical focusing and assume that the system has infinite length in x (out of the page). The magnets are oriented to produce a dipole field B_y with alternating polarity along the axis. Top and bottom iron pieces provide shielding and carry the return flux above and below the assembly. The axial length of the first cell must be about half that of a standard cell to ensure that there is no net drift motion of the beam in x.

At locations far from the entrance, the dipole field has the approximate variation

$$B_y(x,0) \cong B_0 \cos(kx) \tag{1}$$

where $k = L_c/\pi$ and L_c is the magnet length along z. Inspection of Fig. 2 shows that there are B_z field components that have maximum amplitude at the cell boundaries. The dipole fields (B_y) impart an oscillating velocity in the x direction. The resulting $v_x \times B_z$ force provides focusing along y. The B_z components have opposite polarity above and below the vertical axis.

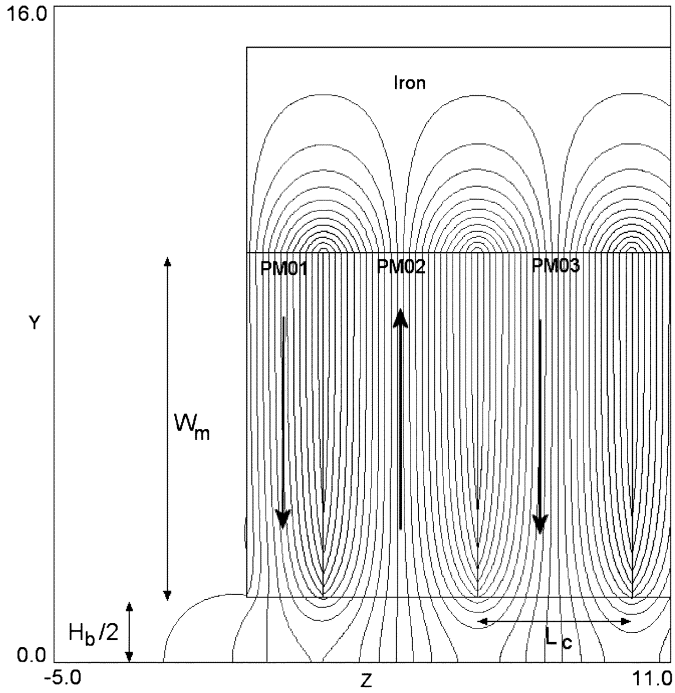

Fig. 2. View of a wiggler magnet array (in a plane normal to x) with dimensions used in the 2-D simulations. (Note that the assembly is symmetric about $y = 0.0$, and only the region $y > 0.0$ is shown.) Bold arrows show the direction of magnetization. Magnetic field lines calculated with the PerMag code. Dimensions in millimeters.

We can, therefore, approximate the field component near $y = 0$ with the expression

$$B_z \cong y f(z). \tag{2}$$

Because there are no current sources, the condition $\nabla \times \mathbf{B} = 0$ holds, or

$$\frac{\partial B_z}{\partial y} = \frac{\partial B_y}{\partial z}. \tag{3}$$

Substitution of (1) and (2) in (3) determines $f(z)$ and gives an expression for the axial component of field

$$B_z(y,z) \cong -kB_0 \sin(kz) y. \tag{4}$$

Canonical momentum is a conserved quantity along the x direction

$$P_x = \gamma m_e v_x - eA_x. \tag{5}$$

The condition $P_{\rm x} = 0$ holds if the electrons enter from a region of zero magnetic flux. The vector potential is related to the dipole field by

$$B_y = \frac{\partial A_x}{\partial z}. \tag{6}$$

Integration of (6) gives

$$A_x = \frac{B_0}{k}\sin(kx). \tag{7}$$

Combining (5) and (7) gives an expression for the velocity along x

$$v_x = \frac{eB_0}{\gamma m_e k}\sin(kz). \tag{8}$$

Taking the vertical magnetic force as $ev_{\rm x}B_{\rm z}$ and introducing beam-field and emittance forces [16], we find the following equation for the envelope half-width Y

$$\frac{d^2Y}{dz^2} \cong -\left(\frac{eB_0\sin(kz)}{\gamma m_e \beta c}\right)^2 Y + K_y + \frac{\varepsilon_y^2}{Y^3}. \tag{9}$$

In (9), $K_{\rm y}$ is the linear generalized perveance

$$K_y = \frac{eJ}{2\varepsilon_0 m_e(\gamma\beta c)^3} \tag{10}$$

where ε_0 is the permittivity of free space. The quantity J in (10) is the line current density of the sheet beam in A/m. The quantity $\varepsilon_{\rm y}$ is the vertical emittance

$$\varepsilon_y \cong Y\Delta\theta_y \tag{11}$$

where $\Delta\theta_{\rm y}$ is the amplitude of the vertical angular divergence. Averaging over z gives the envelope equation for a sheet beam in a 2-D wiggler

$$\frac{d^2Y}{dz^2} \cong -\frac{1}{2}\left(\frac{eB_0}{\gamma m_e \beta c}\right)^2 Y + K_y + \frac{\varepsilon_y^2}{Y^3}. \tag{12}$$

Setting $d^2Y/dz^2 = 0$ gives an approximate condition for a matched beam. For specified values of beam kinetic energy, linear current density and angular divergence, we can calculate the required value of B_0 for a desired beam height.

Equation (12) is identical to the envelope equation for planar-beam focusing in a periodic-permanent-magnet (PPM) system with peak axial field B_0 [16]. Although the focusing forces have the same scaling, the wiggler system has the following advantages.

1) Vacuum fields are confined to the beam transport region.
2) It is not necessary to place iron flux conductors between magnets.
3) Field levels are relatively low in the flux conductors so that they are not saturated.

The implication is that higher values of B_0 can be obtained in a wiggler with the same volume of magnet material.

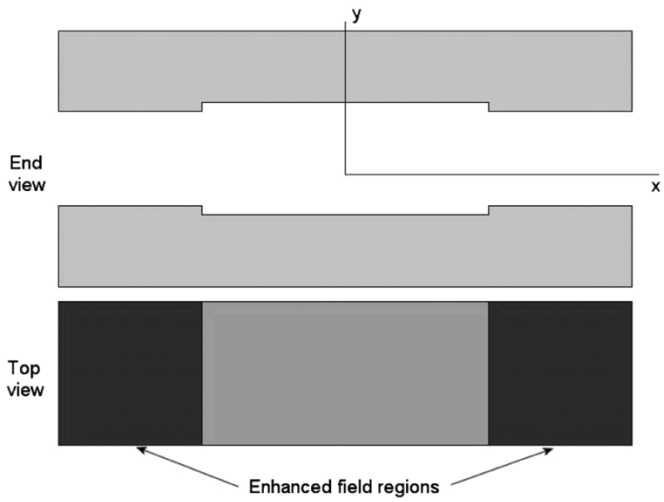

Fig. 3. Shaped wiggler magnets for horizontal (wiggle-plane) focusing.

Horizontal beam focusing will be necessary in the LANL experiments. In the circular-to-planar transformation [14], it is not possible to achieve simultaneous waists in the vertical and horizontal directions at the injection point. As a result, the beam has a small nonzero horizontal envelope angle which adds to the effects of space charge and angular divergence. Although defocusing forces are small compared to those in vertical direction, we expect a significant increase in the beam width over the required interaction length. Several approaches have been suggested for wiggle-plane focusing that involve supplemental focusing magnets or shaped magnet faces [11], [17]–[20]. Fig. 3 shows our approach for planar beam confinement. The wiggler-magnet surfaces facing the beam have a notch giving a small step in the dipole field at the desired beam width [19], [20]. Electrons that drift outward and cross the transition suffer an enhanced inward deflection, reversing the drift direction. This approach has advantages compared to other configurations.

1) All magnets are identical.
2) There are no extra parts or alignment requirements beyond those of a uniform-field wiggler.
3) The effective force approximates a reflecting wall so that confinement is not sensitive to the beam space-charge distribution or magnitude of the field transition.

Fig. 4 demonstrates the focusing mechanism. The illustration shows the orbits of 120-eV electrons moving in the calculated 3-D magnetic field described in Section 4. The notch provides a sharp field transition from $|B_{\rm y}| = 0.426$ T to 0.496 T near $x = \pm 5.0$ mm (at the cell axial cell midplanes). The background color shows $|B_{\rm y}|$ in the plane $y = 0.0$. In Fig. 4(a), electrons enter parallel to the z axis at different displacements in x. All

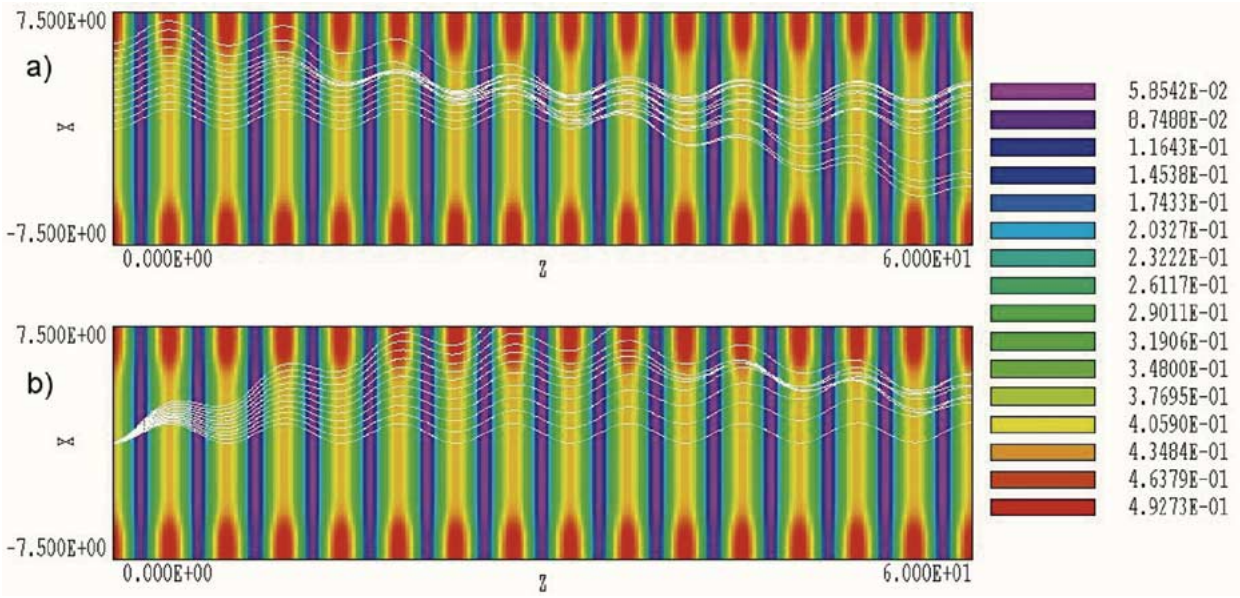

Fig. 4. Horizontal electron orbits projected to the x-z plane in a notched wiggler array. Electron injection energy: 120 keV. Color-coding shows $|B_y|$ in the plane $y = 0.0$. Magnetic field values in T. Dimensions in mm. (a) Injection parallel to the z axis over the reduced-field range in x. (b) Injection at $x = 0.0$ over a range of horizontal angle from $x' = 0.00$ to 0.25 rad.

TABLE II
BASELINE WIGGLER PARAMETERS

Quantity	Symbol	Value
Axial cell length	L_c	4.0 mm
Vertical bore (full height)	H_b	3.2 mm
Assembly full height		30.0 mm
Magnet vertical height	W_m	8.4 mm
Magnet material		NeFeB 35H
Remanence flux density	B_r	1.2 tesla

electrons that start within the reduced-field region are confined. (Note that electrons that enter with displacements $x > 5.0$ mm sense a wiggler field that is uniform in x and are not focused.) Fig. 4(b) shows orbits of electrons injected at $x = 0.0$ over a range of angles from 0.0° to 14.4°. With the given magnetic field values and a cell length of $L_c = 4.0$ mm, the notched wiggler confines 120-keV electrons up to an angle of 9.93° (0.17 radians). This value significantly exceeds the maximum horizontal divergence and envelope angles expected in the LANL experiment.

III. BEAM MATCHING AND VERTICAL FOCUSING

We used the PerMag and Trak codes to study vertical matching of a focused, high-intensity sheet beam into a wiggler array. In the 2-D simulations the system had infinite length in x (the horizontal direction). Table II shows the baseline parameters for the miniature wiggler array. Fig. 2 shows the entrance region to scale and definitions of geometric quantities.

The initial cell had an axial length of $L_c/2 = 2.0$ mm. Beyond this, there were no special provisions to optimize beam matching. The simulation modeled the fringe field region, the first half-cell and fifteen full cells. A flux-excluding boundary for the finite-element solution was located at $z = -5.0$ mm. Fig. 5 shows the variation of the on-axis magnetic flux density $B_y(0, z)$ in the fringe region and over the first few cells. At locations distant from the entrance the peak dipole field was $B_0 = 0.423$ T. The solution for the beam-generated electric fields was performed inside a grounded chamber of dimensions $y_w = \pm 1.00$ mm. The conducting boundaries gave an approximate representation of the image-charge effects of the traveling wave structure.

Following the results of [14], we sought conditions where the beam distribution at $z = 0.0$ mm filled a rectangle in vertical phase-space with dimensions $y_0 = \pm 0.25$ mm and $y_0' = \pm 0.06$ radians. We used a linear current density of $J = 2828$ A/m, consistent with the parameters of Table I. There was a complicating factor in the initiation of model-particle orbits. While we knew the desired distribution at $z = 0.0$ mm, it was essential to start electrons at the solution volume boundary ($z = -5.0$ mm) to ensure that they had canonical momentum $P_x = 0$. Electrons that started at $z = 0.0$ mm exhibited a horizontal drift of 8.0 mm over the 62 mm length of the wiggler array. To ensure the correct match conditions, we created a set of 200

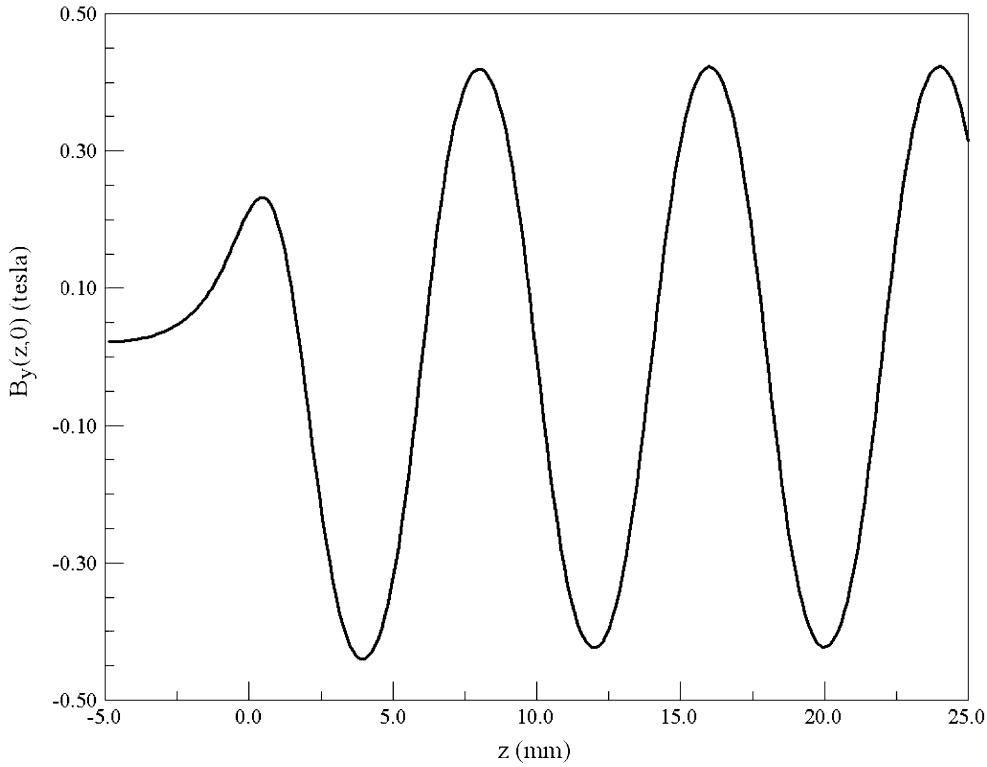

Fig. 5. Variation of $B_y(0,z)$ in the 2-D calculation near the wiggler entrance at $z = 0.0$.

model electrons at $z = 0.0$ mm with the desired phase-space distribution and with average velocity in the $-z$ direction. An initial Trak run was performed with no applied magnetic field to project the particles to $z = -5.0$ mm with self-consistent effects of beam space-charge and current. The momentum vectors were then reversed, and the resulting distribution was used as the input for the main simulation. The procedure yielded a converging beam with $P_x = 0.0$ that reached a height of approximately $y_0 = \pm 0.25$ mm at $z = 0.0$.

Using target values for the beam and focusing system parameters, (12) implies that the peak magnetic field for a match is approximately $B_0 = 0.357$ T. To investigate a range of applied magnetic fields, the baseline PerMag solution was reduced by a scaling factor for the Trak orbit calculations. Reduced values could easily be achieved in physical system by changing magnetic materials (B_r) or reducing W_m. A series of calculations was performed with different values of the scaling factor to seek the best match. The solutions included self-consistent effects of beam-generated fields. Because the orbits were paraxial and the vacuum system was uniform in z, it was sufficient to use the relativistic approximation. Here, the combined effects of beam-generated electric and magnetic forces are contained in the total force expression

$$F_y = -\frac{eE_y}{\gamma^2}. \tag{13}$$

The quantity γ is normally referred to as the relativistic energy factor and E_y is the vertical component of beam-generated electric field. The application of (13) reduces the run time and generally gives higher accuracy than individual calculations of the electric and magnetic fields. Fig. 6 shows magnetic field lines and orbit traces for three cases: 1) under-matched ($B_0 = 0.233$ T); 2) approximately matched ($B_0 = 0.381$ T); and 3) over-matched ($B_0 = 0.508$ T). Note that the vertical scale has been expanded by about $30\times$ to show details of the orbits. Over the large range of applied field, the beam propagated stably through the full system with little growth in envelope width. (Note that the Trak code is capable of modeling envelope instabilities—we did observe the growth of envelope oscillations in simulations with larger values of L_c.) The peak field for the best match was consistent with the prediction of (12). With regard to vertical confinement, the simulations suggest that the focused beam from the transformation system described in [14] can be injected directly into a uniform wiggler array without a special conditioning section. For $B_0 = 0.382$ T, the wiggle amplitude was about ± 1.0 mm. The net horizontal drift was quite small (<0.2 mm) even though no special effort was made in the design of the initial half-length cell.

We made some additional runs to check the effect of variations of remanence magnetic field (B_r) and magnet thickness on vertical containment. Small variations were introduced into the baseline system of Table II with $B_0 = 0.382$ T. Because of the calculation symmetry, the variations applied to both the top and bottom magnets of a set. Manufacturers quoted a typical level for variations of B_r of about $\pm 5\%$ without selection. Assuming that the figure represents a root-mean-squared value, we sampled random values of B_r from a uniform distribution with a width of $\pm 7.1\%$. These values were inserted into PerMag to create the field distribution of Fig. 7(a). The resulting particle orbits are illustrated in Fig. 8(a). The quoted dimension tolerance was about ± 0.05 mm. Again taking the figure as a root-mean-square value, we sampled lengths from a uniform

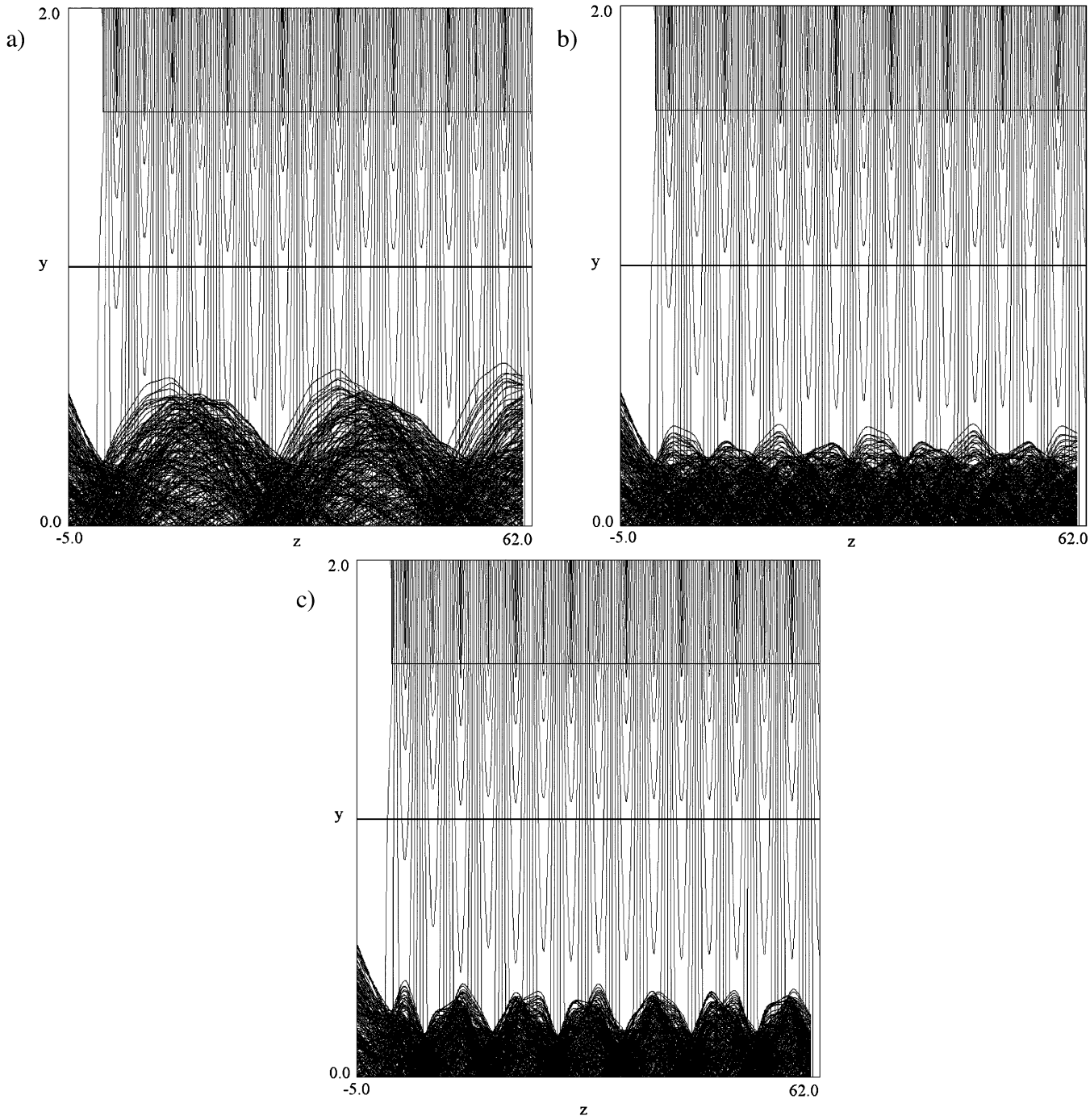

Fig. 6. Model electron orbits and magnetic field lines in the y-z plane for different amplitudes of applied field. Two dimensional simulations with the Trak code include self-consistent effects of beam space-charge and current. Note that there is a vertical magnification of $30\times$. Dimensions in mm. Solid line shows the vacuum chamber boundary at $y = 1.0$ mm. (a) $B_0 = 0.233$ T. (b) $B_0 = 0.381$ T. (c) $B_0 = 0.508$ T.

distribution with boundaries 4.0 ± 0.071 mm. Fig. 7(b) illustrates typical field variations with random differences in magnet thickness while Fig. 8(b) shows beam particle orbits. Both types of errors introduced significant variations in the peak magnetic field. Because the high and low values tended to clump statistically, the effects on beam containment were pronounced. The growth of envelope oscillations comparable to the desired beam height is evident in Fig. 8(a) and (b). To be conservative in the fabrication of the wiggler, we have decided to reduce variations in B_r below the $\pm 5\%$ level by selection and to specify magnet thickness to a tolerance of ± 0.0127 mm. A positive implication of Fig. 7(a) and (b) is that an axial scan of the vertical magnetic field gives a sensitive test of the material and dimensional uniformity of the array.

IV. Horizontal Focusing With Notched Wiggler Magnets

We used the Magnum code [21] to calculate 3-D magnetic fields of a notched wiggler array. In the beam transport region,

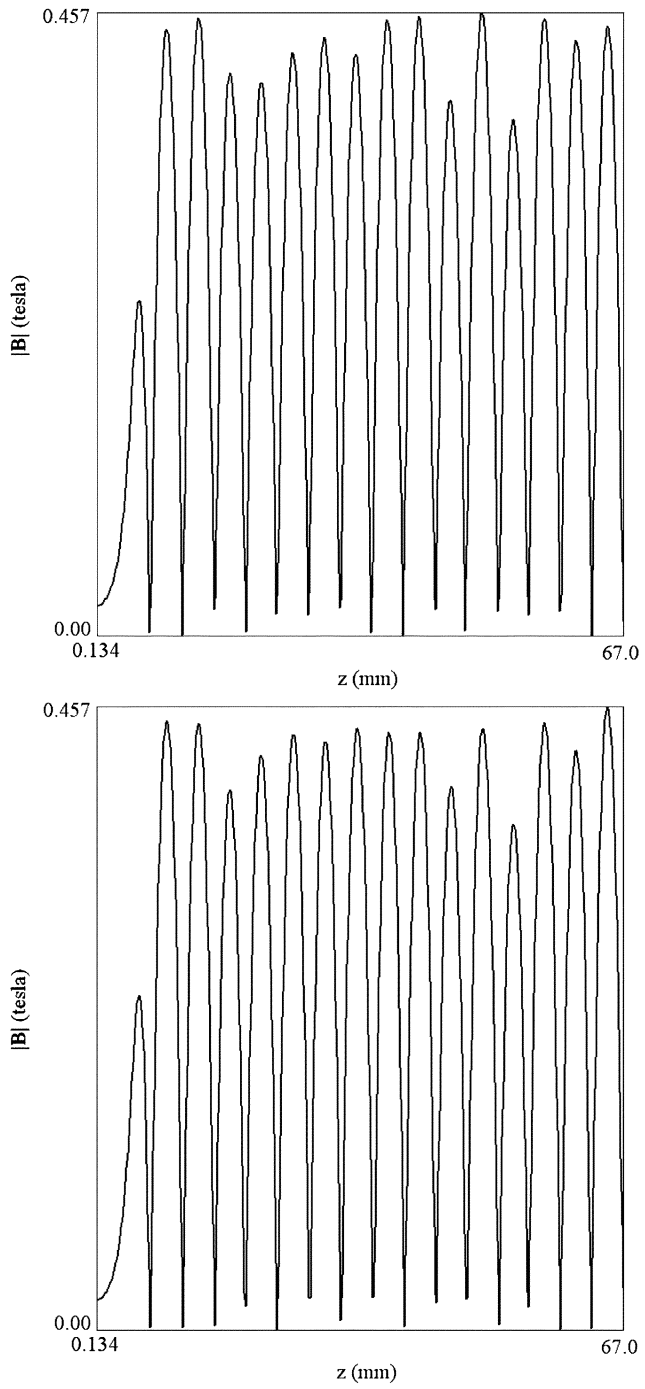

Fig. 7. Scans of $B_{\rm y}(0,z)$ for arrays with random errors of $B_{\rm r}$ and magnet axial thickness (2-D simulations). (a) 5 per cent error in $B_{\rm r}$. (b) 1.25 per cent error in magnet thickness.

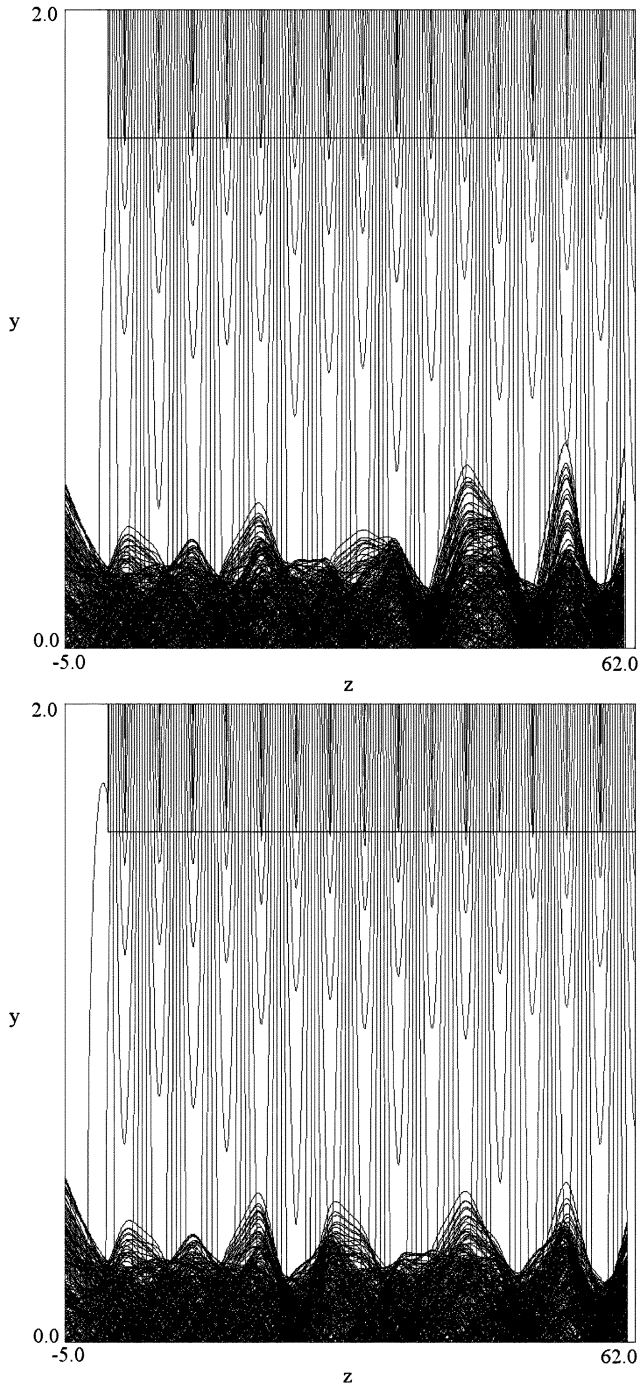

Fig. 8. Model electron orbits and magnetic field lines in the y-z plane using the calculated magnetic fields shown in Fig. 7. Two dimensional simulations with the Trak code including self-consistent effects of beam space-charge and current. Note that there is a vertical magnification of $30\times$. Dimensions in mm. (a) Error in $B_{\rm r}$. (b) Error in magnet thickness.

the magnets had the same vertical dimensions used in the calculations of Section III. The vertical gap between magnets equaled 3.2 mm in the horizontal range $-5.0\,\text{mm} < x < 5.0$ mm and 2.8 mm for $|x| > 5.0$ mm. The simulation system consisted of one half-cell with 2 mm length and 15 cells of length 4.0 mm. For simplicity, a flux-excluding boundary was located at the entrance to the first cell—the simulation did not address matching in the fringe fields at the entrance. Fig. 9 shows a section of the array along with a color-coded representation of $|B_{\rm y}|$ in the plane $y = 0.0$. For clarity, the iron flux return pieces and half of the magnets have been omitted from the plot. On the axial midplane of a cell, the value of $|B_{\rm y}|$ was 0.426 T, close to the result of the 2-D calculation. The value outside the transition was 0.496 T, 16% higher than the central field.

An input distribution of 400 model electrons starting at $z = 0.0$ mm was created with the GenDist program [21]. The 120-keV beam uniformly filled a rectangle in the transverse plane of dimensions $-4.0\ \text{mm} < x < 4.0$ mm and $-0.30\ \text{mm} < y < 0.30$ mm. Injection angles were randomly

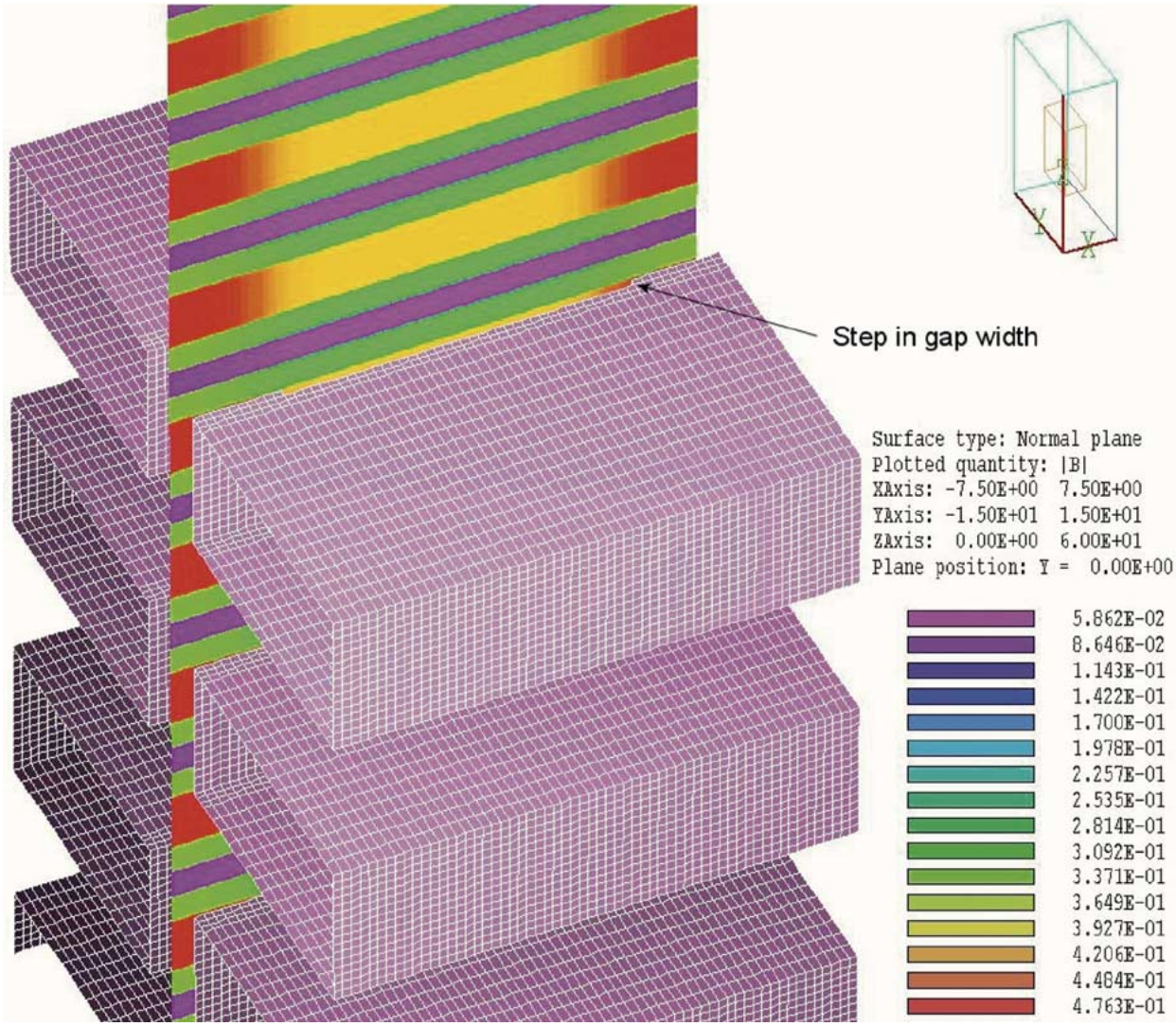

Fig. 9. Three-dimensional magnetic field solution generated by the Magnum code for the notched wiggler simulation. Magnet-face step at $x = \pm 5.0$ mm reduces the full gap-width from 3.2 to 2.8 mm in the outer regions. Color-coded surface shows $|B_y|$ at $y = 0.0$. Iron structures and half of the magnets are omitted for clarity.

assigned in the range -0.06 rad $< x' < 0.06$ rad and -0.06 rad $< y' < 0.06$ rad to created uniform angular divergences in x and y. The injected beam was displaced -1.00 mm in x so that the average horizontal position in the wiggler was at $x = 0.0$ mm. A magnetic-field adjustment factor of 0.90 gave a good vertical beam match, consistent with the prediction of (12) and the results of Section III. In the orbit simulation, the peak vertical field at $x = 0.0$ was 0.383 T. The solution for the beam-generated space-charge electric fields was performed in a grounded chamber with a rectangular cross section. The chamber was uniform in z and had dimensions ± 1.0 mm in the vertical direction and ± 6.0 mm in the horizontal direction. A small vertical element size of $\Delta y = 0.05$ mm was used for good resolution of the beam-generated forces. The simulation employed the relativistic mode (13) to represent the effects of beam-generated magnetic fields. The total current of 22.62 A corresponded approximately to a line current density of $J = 2828$ A/m.

Fig. 10 illustrates results of the simulations. The upper-right plot shows lines of constant beam-generated electrostatic potential at $z = 30.0$ mm with superimposed electron orbits projected to the x–y plane. The orbits combine vertical betatron oscillations with reflection and wiggle motions in the horizontal direction. The plot shows that the beam remains confined in both the horizontal and vertical directions over the full length of the simulation volume with little distortion of the profile. The lower-left plot shows orbits projected to the z-x plane combined with a color-coded representation of $|B_y|$ in the plane $y = 0.0$. The orbit plot shows the wiggle motion and illustrates beam confinement in the horizontal direction. No electrons were lost to the vacuum chamber walls at $x = \pm 6.0$ mm. For comparison, Fig. 11 shows the same type of plot with the beam injected into an un-notched array with uniform magnetic fields in the horizontal direction. The beam expanded under the influence of space-charge forces and emittance. The envelope struck the wall at $z = 25$ mm. Approximately 16% of the beam current was lost to the vacuum chamber at the system exit ($z = 60.0$ mm).

In conclusion, the process of nonlinear focusing by shaped wiggler magnets appears to be robust and tolerant. The system illustrated in Figs. 9 and 10 was an initial estimate based on the

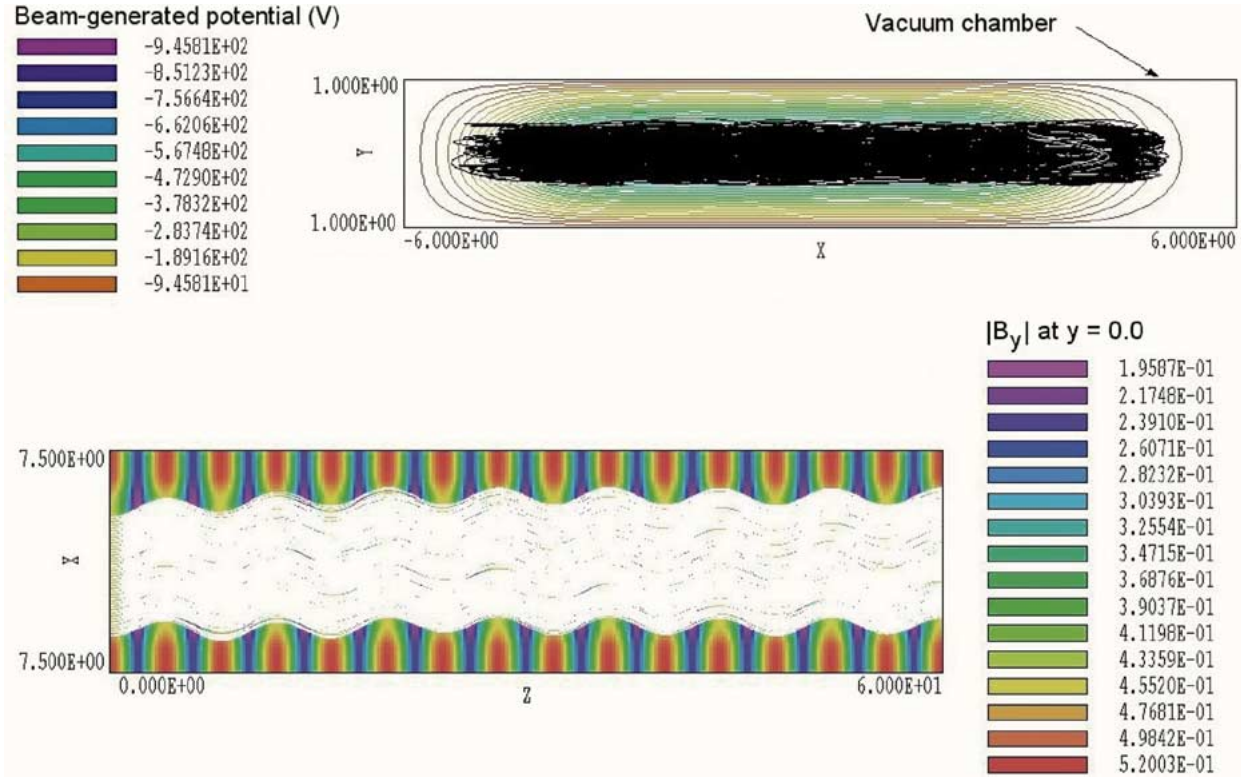

Fig. 10. Three-dimensional simulations of beam transport in a wiggler with shaped magnets. OmniTrak calculation with 400 model electrons includes self-consistent effects of beam space charge and current. Top-right: Contours of beam-generated electrostatic potential at $z = 30.0$ mm (legend at left) with superimposed orbits projected to the x-y plane. Bottom-left: Color-coded plot of $|B_y|$ at $y = 0.0$ (legend at right) with orbits projected to the z-x plane (legend at right). Dimensions in mm. Dashed line shows the walls of the vacuum chamber.

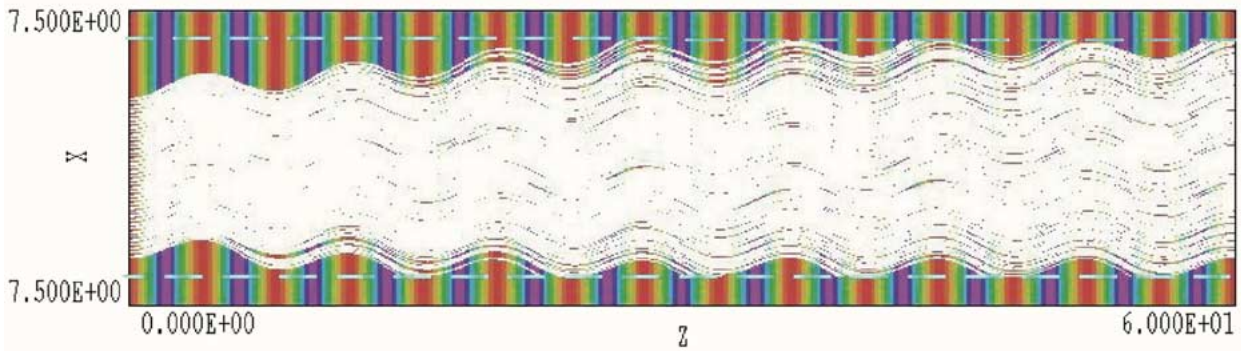

Fig. 11. Three-dimensional simulations of beam transport in a wiggler with un-notched magnets. Color-coded plot of $|B_y|$ at $y = 0.0$ with orbits projected to the z-x plane. Dimensions in mm. Dashed line shows the walls of the vacuum chamber.

2-D results with no optimization. The notched array has the additional virtues that it is easy to fabricate, makes effective use of the magnetic material and is insensitive to the size of the magnet step and details of the beam distribution.

REFERENCES

[1] J. Joe, S. F. Chang, J. E. Scharer, and J. H. Booske, "Linear analysis of sheet beam planar grating and dielectric Cherenkov maser amplifers," *Microw. Opt. Tech. Lett.*, vol. 4, p. 443, 1991.

[2] J. H. Booske and M. A. Basten, "Demonstration via simulation of stable confinement of sheet electron beams using periodic magnetic focusing," *IEEE Trans. Plasma Sci.*, vol. 27, no. 1, pp. 134–135, Feb. 1999.

[3] B. D. McVey, M. A. Basten, and J. H. Booske, "Analysis of rectangular waveguide-gratings for amplifier applications," *IEEE Trans. Microw. Theory Tech.*, vol. 42, no. 6, pp. 995–1003, Jun. 1994.

[4] J. Joe, L. J. Louis, J. E. Scharer, J. H. Booske, and M. A. Basten, "Experimental and theoretical investigations of a rectangular grating structure for low-voltage traveling wave tube amplifiers," *Phys. Plasmas*, vol. 4, p. 2707, 1997.

[5] E. R. Colby, G. Caryotakis, W. R. Fowkes, and D. N. Smithe, "W-band sheet beam Klystron simulation," in *High-Energy Density Microwaves, Conf. Proc.*, vol. 474, R. M. Phillips, Ed.. New York, 1998, p. 74.

[6] G. Caryotakis, "NLC Klystron R&D," in *5th Workshop High Energy Density High-Power RF, Conf. Proc.*, vol. 625, B. Carlsten, Ed.. New York, 2001, p. 1.

[7] P. B. Wilson, "RF power sources for 5–15 TeV linear colliders," presented at the Int. Workshop RF Pulsed Sources Linear Colliders, Palo Alto, CA, 1996.

[8] M. E. Read *et al.*, "Gridded sheet beam gun for a sheet beam Klystron," in *Proc. IR MM Wave Conf.*, Portland, OR, Sep. 2002.

[9] B. E. Carlsten, "Pierce Grain Analysis for a sheet beam in a rippled waveguide traveling wave tube," *Phys. Plasmas*, vol. 8, p. 4585, 2001.

[10] M. A. Basten, J. H. Booske, and J. Anderson, "Magnetic quadrupole formation of elliptical sheet electron beams for high-power microwave devices," *IEEE Trans. Plasma Sci.*, vol. 22, no. 5, pp. 960–966, Oct. 1994.
[11] M. A. Basten and J. H. Booske, "Two-plane focusing of high-space-charge sheet electron beams using periodically cusped magnetic fields," *J. Appl. Phys.*, vol. 85, p. 6313, 1999.
[12] B. E. Carlsten, L. M. Earley, W. B. Haynes, and R. M. Wheat, "Design of high-power MM-wave traveling–wave tubes," in *5th Workshop on High Energy Density High-Power RF, Conf. Proc.*, vol. 625, B. Carlsten, Ed.. New York, 2001, p. 117.
[13] B. E. Carlsten, S. J. Russell, L. M. Earley, J. M. Potter, P. Ferguson, and S. Humphries Jr., "MM-wave source development at Los Alamos," in *6th Workshop on High Energy Density and High-Power RF, Berkeley Springs, Conf. Proc.*, vol. 691, S. Gold and G. Nusinovich, Eds. New York, 2003, p. 349.
[14] S. Humphries, S. Russell, B. Carlsten, L. Earley, and P. Ferguson, "Circular-to-planar transformation of high–perveance electron beams by asymmetric solenoid lenses," *Phys. Rev. Spec. Topics Acc. Beams*, vol. 7, p. 060 401, 2004.
[15] T. C. Marshall, *Free-Electron Lasers*. New York: Macmillan, 1985.
[16] S. Humphries, *Charged Particle Beams*. New York: Wiley, 1990, sec. 9.1.
[17] M. A. Basten, J. H. Booske, J. Anderson, and J. E. Scharer, "Formation and transport of sheet electron beams and multi-beam configurations for high-power microwave devices; Intense microwave pulses III," *Proc. Soc. Photo-Optical Inst. Engr.*, vol. 2557, p. 262, 1995.
[18] E. T. Scharlemann, "Wiggler plane focusing in linear wigglers," *J. Appl. Phys.*, vol. 58, p. 2154, 1985.
[19] C. M. Fortgang, "A pure permanent magnet—Two plane foucsing—Tapered wiggler for a high average power FEL," *Nucl. Instrum. Methods*, vol. 58, p. 2154, 1997.
[20] B. Shepherd and J. Clarke, "Magnet Design of a Focusing Undulator for Alpha-X," Daresbury Laboratory, 2003. unpublished.
[21] PerMag, Trak, Magnum, Gendist and OmniTrak Codes, Copyright Field Precision [Online]. Available: http://www.fieldp.com
[22] B. E. Carlsten, "Small signal analysis and particle-in-cell simulations of planar dielectric Cherenkov masers for use as high-frequency, moderate-power broadband amplifiers," *Phys. Plasmas*, vol. 9, p. 1790, 2002.
[23] B. E. Carksten, "Modal analysis and gain calculations for a sheet beam in a ridged waveguide slow-wave structure," *Phys. Plasmas*, vol. 9, p. 5088, 2002.

Stanley Humphries (M'75–SM'90–F'93) received the B.S. degree in physics from the Massachusetts Institute of Technology, Cambridge, and the Ph.D. degree in nuclear engineering from the University of California, Berkeley.

He is a Professor Emeritus in the Department of Electrical and Computer Engineering, the University of New Mexico, Albuquerque, and President of Field Precision, Albuquerque, NM, an engineering software company. He spent the first part of his career as an experimentalist in the fields of plasma physics, controlled fusion, and charged particle acceleration. A notable contribution was the creation and demonstration of methods to generate and to transport intense pulsed ion beams. His current work centers on simulations of electromagnetic fields, biomedical processes, and material response at high pressure and temperature. He is the author of over 150 journal publications and the textbooks *Principles of Charged-Particle Acceleration* (Wiley, New York, 1986), *Charged Particle Beams* (Wiley, New York, 1990), and *Field Solutions on Computers* (CRC, Boca Raton, FL, 1997).

Dr. Humphries is a Fellow of the American Physical Society.

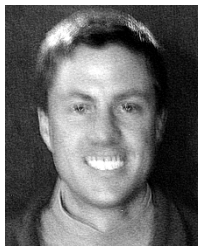

Steven Russell received the Ph.D. degree in physics for Michigan State University, East Lansing, in 1998 with a focus in accelerator beam physics.

He joined Los Alamos as a Student during the summers of 1990 and 1991 to work on the Advanced Free Electron Laser (AFEL) project. In 1992, he joined Los Alamos as a Graduate Research Assistant for an extended stay to work on his Ph.D. thesis. Upon graduating, he was hired as Staff at Los Alamos and has continued his research in accelerator physics, specifically on the behavior of electron beams. Since 2002, he has worked to develop sheet electron beams for mm-Wave vacuum tube devices.

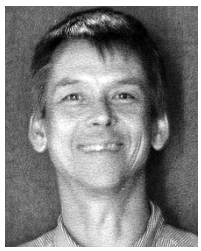

Bruce Carlsten received the B.S. degree in physics from the University of California, Los Angeles, and the Ph.D. degree in electrical engineering from Stanford University, Stanford, CA, in 1979 and 1985, respectively.

In 1982, he joined the Los Alamos National Laboratory, Los Alamos, NM, and has published research in the areas of electron beam emittance growth and compensation, intense electron-beam physics, electron beam bunch compression, coherent synchrotron radiation, RF and induction accelerators, sheet beam transport, klystrons, and traveling-wave tubes. His main interests are numerically modeling electron beam dynamics and RF generation, and designing and operating beam and RF experiments. He is currently a Project Leader at Los Alamos for the sheet beam traveling-wave tube development program. He has over 60 refereed publications and six patents.

Dr. Carlsten received the 1999 U.S. Particle Accelerator School Prize for Achievement in Accelerator Physics and Technology for his work on emittance compensation. He received a 1994 Los Alamos National Laboratory Distinguished Performance Award for his work on bunch compression.

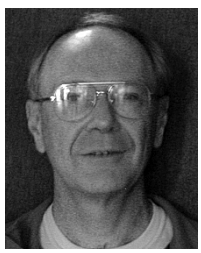

Lawrence Earley received the M.S. degree in electrical engineering, from Stanford University, Stanford, CA, in 1979 and the degree of engineer in electrical engineering from Stanford University as part of the Air Force Thermionic Engineering Research (AFTER) Program, in 1981.

He has over 25 years experience in high-power microwave generation at Los Alamos National Laboratory, Sandia National Laboratories, and Hughes Aircraft Company, EDD, including developing high-power microwave generators (magnetrons, backward wave oscillators, MILOs, vircators, TWTs, FEMs and klystrons). He has extensive experience with pulsed power, electron beams and RF diagnostics, and precision measurements for frequencies up to 300GHz. He has extensive experience on RF accelerator structures including RFQs, side-coupled, drift tube linacs, and LIAs. He has over 25 publications in the field of RF, microwaves and pulsed power.